ATATÜRK ÜNİVERSİTESİ YAYINLARI
ATATURK UNIVERSITY PUBLICATIONS

Research Article *Araştırma Makalesi* DOI: 10.5281/zenodo.14344182

Investigation of Photo-Electrical Properties in (Fe_2O_3-G)/n-Si Device

(Fe_2O_3-G)/n-Si Cihazında Foto-Elektriksel Özelliklerin İncelenmesi

Elif DAŞ [1,2]
[1]*Department of Physics, Science Faculty, Atatürk University, Erzurum, Türkiye*

[2]*Department of Nanoscience and Nanoengineering, Graduate School of Natural and Applied Science, Atatürk University, Erzurum, Türkiye*

Gamze BOZKURT
Technology Transfer Implementation and Research Center, Erzurum Technical University, Erzurum, 25050, Türkiye

Abstract

This study focuses on synthesizing iron oxide-graphene (α-Fe2O3-G) composite materials and evaluating their performance in devices constructed on n-type silicon (n-Si) semiconductors under dark and illuminated conditions. Key electrical parameters such as the ideality factor (n = 2.59), barrier height (Φ_b = 0.74 eV), and series resistance (R_s = 70 kΩ) were determined using Thermionic Emission (TE) and Norde methods from I-V measurements taken in the dark. The device's photoelectrical properties were further examined under illumination, revealing that the Fe_2O_3-G/n-Si device exhibits self-powered behavior, operating without an external power source. The device achieved a maximum ON/OFF ratio of 32496, a specific detectivity (D^*) of 26.6 Jones at 0 V, and a maximum responsivity (R) of 98 mAW^{-1} at -2 V. These results highlight the device's potential for efficient photodetection, particularly in self-powered applications.

Keywords: I-V characteristic, Norde method, Photosensitive device, Micro-emulsion method

Öz

Bu çalışma, demir oksit-grafen (α-Fe_2O_3-G) kompozit malzemelerin sentezlenmesine ve bunların n-tipi silisyum (n-Si) yarıiletkeni ile oluşturulan cihazlardaki performanslarının hem karanlık hem de aydınlık koşullardaki değerlendirilmesine odaklanmaktadır. İdealite faktörü (n= 2,59), bariyer yüksekliği (Φ_b = 0,74 eV) ve seri direnç (R_s = 70 kΩ) gibi elektriksel parametreler karanlıkta alınan I-V ölçümlerinden Termiyonik Emisyon (TE) ve Norde yöntemleri kullanılarak belirlenmiştir. Cihazın fotoelektrik özellikleri aydınlatma altında da incelenmiş ve Fe_2O_3-G/n-Si cihazının harici bir güç kaynağı olmadan çalışarak kendi kendine güç sağlama davranışı sergilediği ortaya çıkmıştır. Aygıt, 0 V'ta maksimum ON/OFF oranına (32496), spesifik dedektiviteye (D^*, 26,6 Jones) ve -2 V'ta da maksimum duyarlılığa (R, 98 mAW^{-1}) ulaşmıştır. Bu sonuçlar, cihazın özellikle kendi kendine güç sağlayan uygulamalarda verimli ışık algılama potansiyeline sahip olduğunu vurgulamaktadır.

Anahtar Kelimeler: I-V karakteristiği, Norde metodu, Işığa duyarlı cihaz, Mikro-emülsiyon yöntemi

Corresponding Author/ Sorumlu Yazar:
G. BOZKURT
E-mail: gamze.bozkurt@erzurum.edu.tr

Received/ Geliş Tarihi 05.08.2024
Accepted/Kabul Tarihi 31.10.2024
Publication Date/ Yayın Tarihi 12.12.2024

Cite this article
Daş, E. & Bozkurt G. (2024) *Investigation of Photo-Electrical Properties in (Fe2O3-G)/n-Si Device*. *Journal of Anatolian Physics and Astronomy, 3*(2), 62-74.

Introduction

Photodetectors are essential optical devices that transform light into electrical signals (Ramakrishnan et al., 2023; Talebi & Eshghi, 2023). Self-powered photodetectors, which do not require an external power source, have become highly significant in the field of optoelectronics (Kim et al., 2024). Their appeal lies in their high performance, low production costs, and stability. The selection of suitable materials and fabrication techniques is crucial to achieving these benefits (Sarkar & Kumar, 2024).

Metal oxide nanoparticles (MO NPs), particularly iron oxide, play a vital role in optoelectronic technology (Saleem et al., 2023). Iron oxide exists in several forms, including hematite (α-Fe_2O_3), maghemite (γ-Fe_2O_3), and magnetite (Fe_3O_4) (Can et al., 2012). Among them, hematite is known for its stability and suitable band gap for visible light absorption, making it an excellent candidate for photodetector applications (Ghobadi et al., 2019). The inclusion of α-Fe_2O_3 in photodetectors enhances their photoresponse and stability due to its excellent chemical stability, high absorption coefficient, and environmentally friendly nature (Wang et al., 2023).

The synthesis of α-Fe_2O_3 NPs can be achieved through various methods, with the microemulsion method being particularly effective (Han et al., 2011; Muhajir et al., 2019). This method involves creating a microemulsion—a mixture of water, oil, and surfactant—to produce NPs with controlled size and morphology (Li & Park, 1998). The microemulsion technique offers advantages such as simplicity, low cost, and the ability to produce uniform NPs, which are essential for consistent optoelectronic device performance.

Incorporating graphene into composites with MO NPs, such as α-Fe_2O_3, brings additional benefits (Sun et al., 2015; Lu et al., 2019). Graphene, a single layer of carbon atoms arranged in a hexagonal lattice, is known for its exceptional electrical conductivity, mechanical strength, and high surface area (Yurtcan & Daş, 2018; Daş & Yurtcan, 2022). When combined with α-Fe_2O_3 NPs, graphene enhances the charge transport properties, increases the surface area for light absorption, and improves the overall stability of the composite (Alan et al., 2018; Idisi et al., 2023). These enhancements lead to higher sensitivity, faster response times, and greater efficiency in photodetectors.

In this study, we synthesized α-Fe_2O_3-graphene (Fe_2O_3-G) composite materials and fabricated them into thin films on n-type silicon wafers to investigate their impact on device performance. The primary electrical parameters were determined using the Thermionic Emission (TE) theory and the Norde method, which provided insights into the barrier height, ideality factor, and series resistance of the devices. Furthermore, we evaluated the optoelectronic performance of the Fe_2O_3-G composite-based devices by measuring key characteristics such as the ON/OFF ratio, responsivity (R), and specific detectivity (D*) under white light illumination. By systematically analyzing the electrical and optoelectronic parameters, this study provides a detailed understanding of the potential advantages and limitations of Fe_2O_3-G composites in photodetector applications.

Experimental Procedure

Materials

Iron (III) chloride ($FeCl_3$), sourced from the Merck Company, was used as the precursor in this study. The surfactant dioctyl sulfosuccinate sodium salt (AOT), along with 1-butanol, n-heptane, and sodium hydroxide (NaOH), were acquired from Sigma-Aldrich Company in analytical grade. Graphene was supplied by the Nanografi Company (Türkiye). Additionally, during the device fabrication process, an n-type silicon substrate with a resistivity between 1 and 10 Ωcm, a thickness of about 280 μm, and a (100) orientation was used. The surface of the silicon substrate underwent a thorough cleaning procedure.

Material Synthesis

α-Fe_2O_3 material was produced using the microemulsion technique, as documented in prior research (Bozkurt, 2020). This technique was chosen for its effectiveness in generating NPs with uniform size and morphology, which are essential for achieving consistent performance in device applications. Following the synthesis of α-Fe_2O_3 NPs, a mixture of graphene and α-Fe_2O_3 NPs was prepared in a mortar to form the Fe_2O_3-G composite. This was achieved using a 1:0.5 weight ratio,

thoroughly grinding the components in the mortar until a homogeneous mixture was obtained.

Device Fabrication

Initially, the n-type Si substrate was cleaned using the established "Radio Corporation of America (RCA) chemical cleaning processes" (Güllü et al., 2008). Subsequently, a layer of pure aluminum (approximately 120 nm thick) was evaporated onto the unpolished surface of the n-Si wafer at a pressure of $2x10^{-6}$ Torr. The wafer was then annealed at 450 °C for 10 minutes in a nitrogen atmosphere to prevent oxidation on the polished surface. In the next step, the Fe_2O_3-G composite was dissolved in a water/ethanol mixture and applied to the polished surface of the n-Si wafer using the spin coating technique at 1500 rpm, forming a film layer. The coated wafer was left to dry at room temperature overnight. For electrical measurements, gold (Au) dot contacts (with an area of 7.85 x 10^{-3} cm^2) were evaporated onto the Fe_2O_3-G film using the same system employed for the Al back contact. The device design is illustrated in Figure 1. The electrical and photoelectrical properties of the Fe_2O_3-G/n-Si device were examined by using a Keithley sourcemeter at room temperature under both ambient conditions and 1 sunlight intensity.

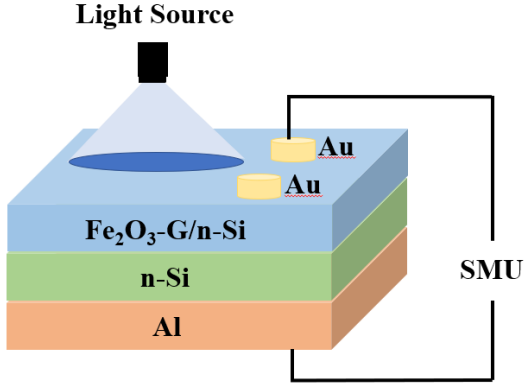

Figure 1. Schematic illustration of the prepared device architecture

Additionally, an Au/n-Si/Al device without Fe_2O_3-G NPs was also fabricated for comparison. This allowed for a detailed assessment of how integrating Fe_2O_3-G affected the device's electrical properties.

Results and Discussion

Some Physical Properties of the Fe_2O_3-G Material

The crystal structure of the Fe_2O_3-G composite was examined through X-ray diffraction (XRD) using a Rigaku Miniflex diffractometer equipped with a Cu Kα radiation source (λ = 1.5406 Å). The XRD pattern displayed distinct peaks corresponding to α-Fe_2O_3, confirming the presence of hematite (α-Fe_2O_3) NPs within the composite material (Bozkurt, 2020), as shown in Figure 2. However, the absence of diffraction peaks for the crystalline phase of graphene could be attributed to the limited amount of graphene mixed with the α-Fe_2O_3 NPs. This lack of peaks may also result from a significant number of α-Fe_2O_3 NPs overlapping on the surface of the graphene (Gao et al., 2022), obscuring the detection of its characteristic peaks in the XRD analysis.

To examine the surface morphology and elemental composition of the Fe_2O_3-G/n-Si structure, SEM and EDS analyses were conducted, as shown in Figure 3. The SEM image reveals a granular texture with irregularly shaped particles, indicating a distinct morphology compared to the previously reported plain Fe_2O_3 structure (Bozkurt, 2020). The incorporation of graphene likely contributes to this altered morphology, promoting the formation of a more interconnected and porous network.

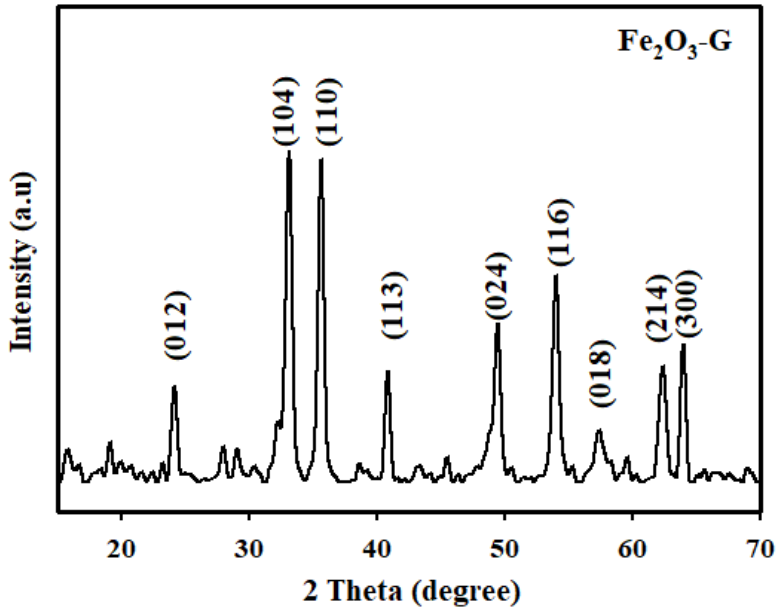

Figure 2. XRD pattern of Fe_2O_3-G material

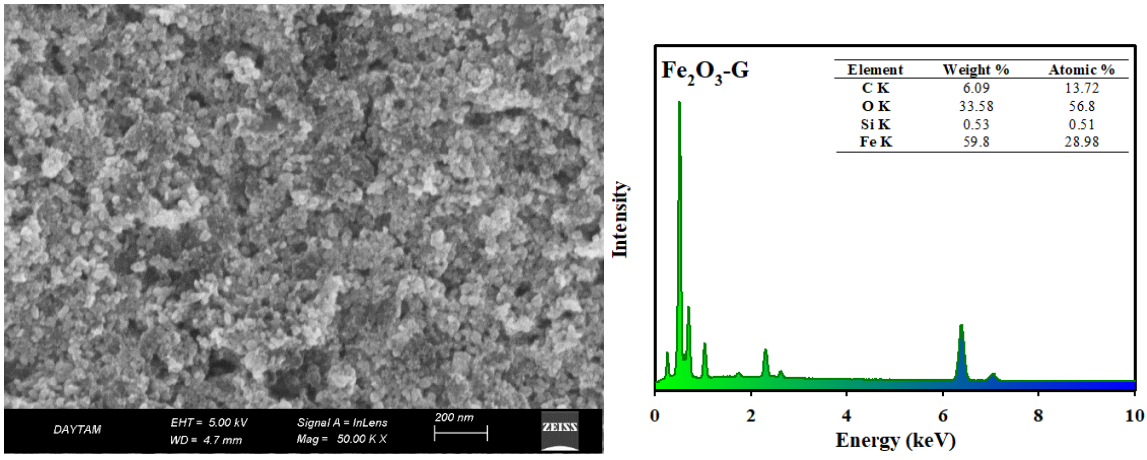

Figure 3. SEM image and the EDS spectrum of Fe_2O_3-G/n-Si structure

Additionally, the EDS analysis confirmed the presence of Fe, C, O, and Si elements in the structure. The slight detection of Si is attributed to the underlying silicon substrate, while the pronounced C peaks confirm the successful incorporation of graphene. The Fe and O peaks correspond to the Fe_2O_3 component, further validating the composition of the composite structure. The EDS results highlight the effective integration of graphene into the Fe_2O_3 matrix, contributing to the material's unique properties.

A UV-Vis absorption analysis was performed to evaluate the optical properties of the Fe_2O_3-G composite. The absorbance spectrum exhibited a wide range of absorption from approximately 300 to 800 nm, indicating strong light absorption across the visible spectrum, which is characteristic of Fe_2O_3-based materials. To determine the band gap, the Tauc plot was employed, and the band gap energy was calculated to be around 2 eV. This value is consistent with the band gaps typically reported in the literature for Fe_2O_3-G composites, which generally fall between 1.9 and 2.2 eV (Abdel-Salam et al., 2022; Idisi et al., 2023), confirming the effectiveness of the composite for optoelectronic and photocatalytic applications. The result aligns well with the expected electronic properties, indicating successful synthesis and integration of the materials.

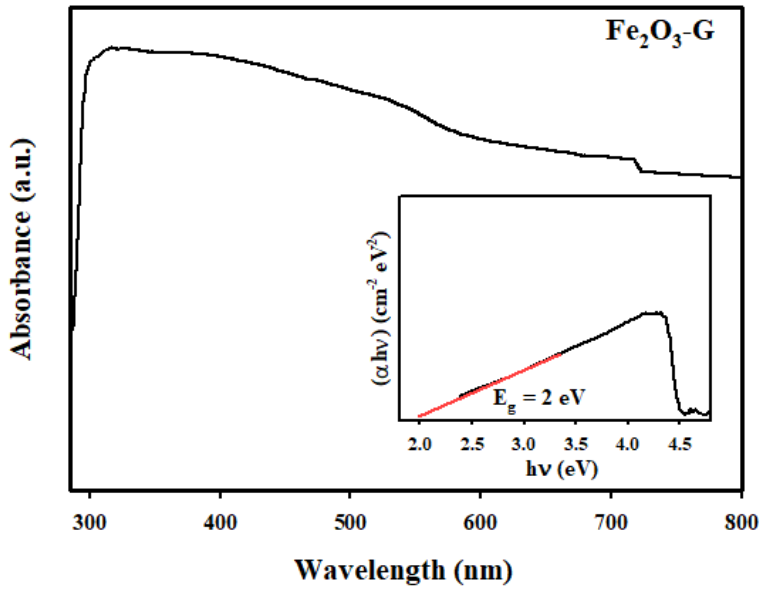

Figure 4. UV-Vis spectra of Fe_2O_3-G composite: Inset shows the Tauc plot of the material

Electro-Optical Properties of the Fe_2O_3-G/n-Si Device Structure

In this study, the devices' current-voltage (I-V) responses were evaluated under two distinct conditions: first, in a dark environment to establish baseline characteristics, and second, under an illumination condition (a visible light source with an intensity of 100 mW/cm^2, equivalent to 1 sun intensity).

Figure 5 shows the I-V curves of the reference (Au/n-Si/Al) and Fe_2O_3-G/n-Si devices in a dark environment. Both devices exhibit excellent rectifying characteristics with an exponential increase in the forward bias region. The fundamental principles of thermionic emission (TE) theory can be utilized to evaluate the electrical parameters of this kind of diode (Orhan et al., 2020; Daş et al., 2021). According to the thermionic emission (TE) theory, the relationship between current (I) and voltage (V) is described as follows (Gupta et al., 2009):

$$I = I_0\left[exp\left(\frac{qV}{nkT}\right) - 1\right] \quad (1)$$

with

$$I_0 = AA^*T^2exp(-q\Phi_b/kT) \quad (2)$$

where I_0 represents the reverse bias saturation current, q is the electronic charge, V is the applied voltage, n is the ideality factor of the diode, k is the Boltzmann constant, T is the temperature in Kelvin, A is the diode area (7.85x10^{-3} cm^2), and A^* is the Richardson constant (112 A/cm^{2}K^2 for n-Si), and Φ_b is the barrier height (Aydoğan et al., 2010).

By rearranging the above equations, the Φ_b and the n can be calculated using the following formulas:

$$\Phi_b = \frac{kT}{q} ln\left(\frac{AA^*T^2}{I_0}\right) \quad (3)$$

$$n = \frac{q}{kT}\left(\frac{dV}{dIn\,I}\right) \quad (4)$$

The ideality factors (n) for the fabricated diodes were found to be 2.03 for the reference device and 2.59 for the Fe_2O_3-G/n-Si device. These values, being greater than one, suggest that both diodes exhibit non-ideal behavior. This non-ideal behavior can be attributed to several factors, including significant surface leakage currents, a high density of recombination

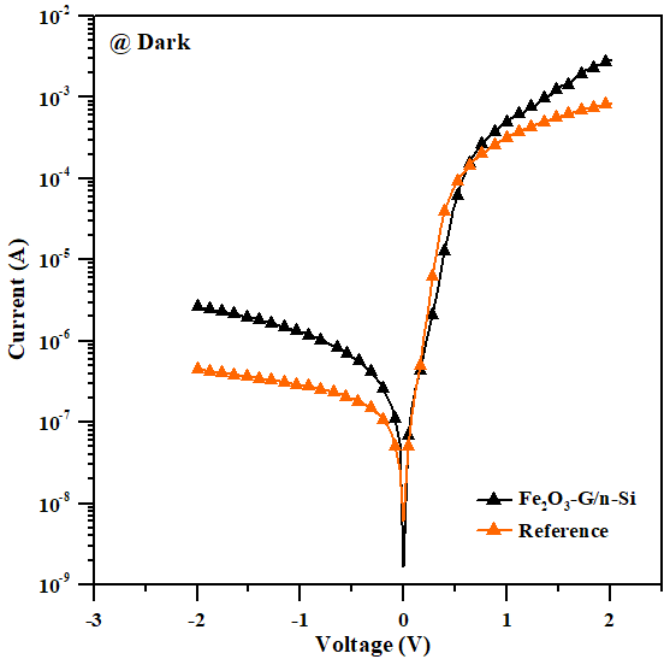

Figure 5. I-V characteristics of the reference and the Fe_2O_3-G/n-Si devices

centers within the depletion region, a high density of interface states, and increased series resistance (Middya et al., 2014; Yıldırım & Daş, 2023). These factors collectively contribute to deviations from the ideal diode behavior, affecting the overall performance of the devices. Additionally, the barrier heights for both devices were determined to be 0.74 eV. The obtained results were tabulated in Table 1.

Table 1. Main electrical parameters of the reference and Fe_2O_3-G/n-Si devices at dark ambient

Reference device					**Fe_2O_3-G/n-Si**				
TE method			**Norde**		**TE method**			**Norde**	
I_0 (x10^{-8} A)	**n**	**Φ_b (eV)**	**Φ_b (eV)**	**Rs (kΩ)**	**I_0 (x10^{-8} A)**	**n**	**Φ_b (eV)**	**Φ_b (eV)**	**Rs (kΩ)**
2.49	2.03	0.74	0.74	490	3.27	2.59	0.74	0.74	70

The elevated ideality factor and the downward concavity observed in the forward bias I–V characteristics at high applied voltages suggest that series resistance (R_s) significantly impacts the device's performance. To address this, Norde developed a method for estimating both the R_s and the Φ_b of diodes (Norde, 1979). Norde's approach involves using a specific function, which can be expressed as follows (Norde, 1979):

$$F(V) = \frac{V}{\gamma} - \frac{kT}{q} ln\left(\frac{I(V)}{AA^*T^2}\right) \quad (5)$$

where γ is an integer greater than the n from the TE theory and the Φ_b can be derived from the Norde function using the following formula (Norde, 1979):

$$\Phi_b = F(V_{min}) + \frac{V_{min}}{\gamma} - \frac{kT}{q} \quad (6)$$

where V_{min} refers to the minimum forward biased value in Norde's function, $F(V)$. Additionally, the R_s value can be determined from Norde's functions as follows (Norde, 1979):

$$R_s = \frac{kT(\gamma - n)}{qI} \quad (7)$$

where I is the current value that corresponds to the minimum value of Norde's function. Figure 6 presents the variation

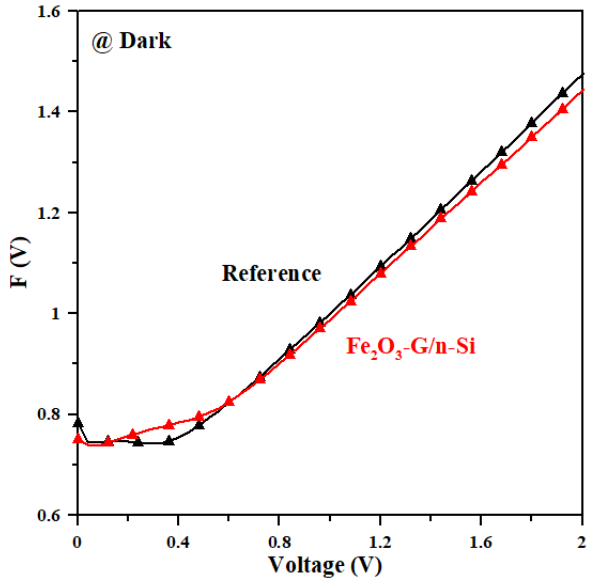

Figure 6. *F(V)* versus *V* plots for the reference and the Fe_2O_3-G/n-Si devices

of Norde's function with the applied voltage for the manufactured devices. Additionally, Table 1 provides the calculated values for the R_s and Φ_b. The results indicate that the Φ_b values derived from both traditional I-V analysis and the Norde approximation are identical. On the other hand, the R_s value of the Fe_2O_3-G/n-Si device is found to be lower than that of the reference device. This can be attributed to several factors. Firstly, the incorporation of Fe_2O_3 and graphene likely enhances the electrical conductivity and charge carrier mobility within the device. Graphene, known for its excellent electrical properties, provides a conductive pathway that reduces resistance. Additionally, the Fe_2O_3 NPs may facilitate better contact at the interfaces, improving the overall efficiency of charge transfer. This synergistic effect between Fe_2O_3 and graphene likely contributes to the reduced R_s, thereby enhancing the device's performance.

Furthermore, the I-V characteristics of the Fe_2O_3-G/n-Si device were analyzed under illumination to investigate their photoelectrical properties, as illustrated in Figure 7. The figure demonstrates that illumination significantly increased the dark current in the negative bias region while having minimal impact on the current in the positive bias region. In photodiodes and photodetectors, this type of I-V characteristic is commonly observed. This behavior therefore suggests that the fabricated device has the potential to be used as an effective photodetector. The high current observed under reverse bias is due to the formation of photogenerated electron-hole pairs and their separation by the internal electric field in the depletion region, which enhances carrier drift and thus increases the photocurrent. Additionally, it is evident that the Fe_2O_3-G/n-Si device demonstrates self-powered behavior, meaning it operates without the need for an external power source.

The ON/OFF ratio of a heterojunction photodetector indicates the device's responsiveness to incident light (Yıldırım & Daş, 2023). It is a crucial parameter that reflects the difference between the photocurrent generated when the device is illuminated (ON state) and the dark current when no light is present (OFF state). A high ON/OFF ratio is desirable as it signifies strong light sensitivity and effective suppression of dark current, leading to better detection accuracy. This ratio also provides insights into the signal-to-noise ratio of the device, which is vital for applications requiring precise light detection. Figure 8 and Table 2 show the variation of the ON/OFF ratio of the Fe_2O_3-G/n-Si device as a function of applied voltage. As light intensity increases, the ON/OFF ratio of the device improves, reflecting enhanced sensitivity to light. Conversely, the ratio decreases with increasing applied voltage. Specifically, the highest ON/OFF ratio is achieved at 0 V, indicating optimal performance at this voltage. In contrast, the ratio diminishes at -2 V, suggesting that higher reverse bias reduces the device's effectiveness in distinguishing between light and dark states. This behavior underscores the importance of optimizing the applied voltage to balance the device's sensitivity and performance.

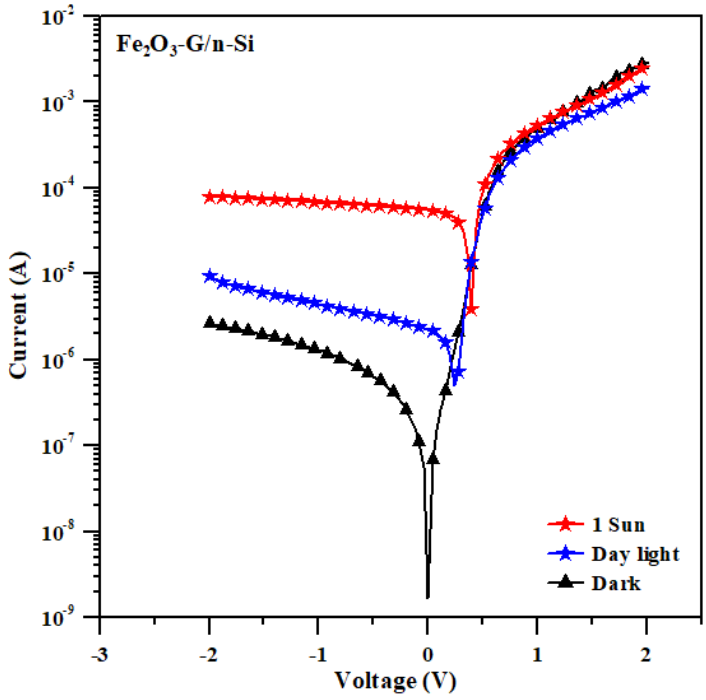

Figure 7. I-V characteristics of the Fe_2O_3-G/n-Si device under illumination

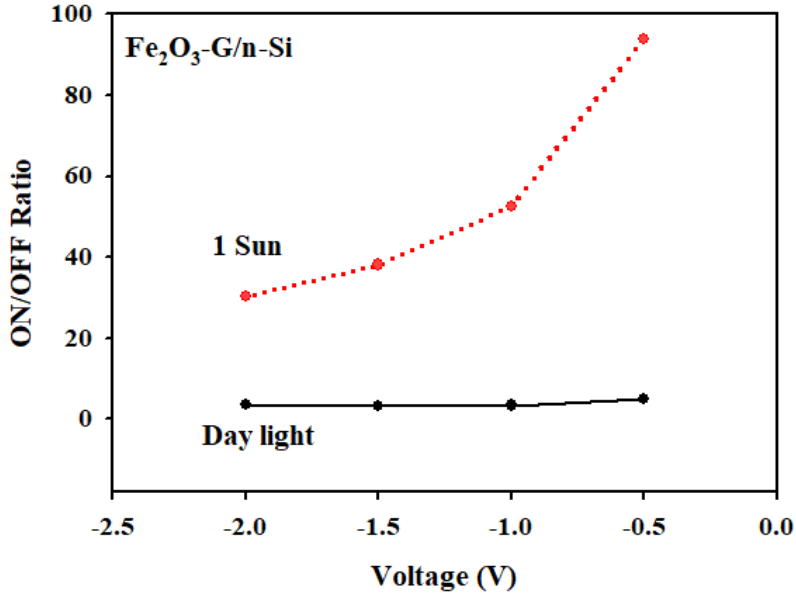

Figure 8. Variation of the ON/OFF ratio of the Fe_2O_3-G/n-Si device as a function of applied voltage

Table 2. ON/OFF ratios of the Fe_2O_3-G/n-Si device for different applied voltages

Device	Ambient	ON/OFF Ratio				
		0V	- 0.5V	-1V	-1.5 V	-2V
Fe_2O_3-G/n-Si	Day light	1334	4.9	3.4	3.1	3.6
	1 Sun	32496	93.7	52.6	38.1	30.3

The efficiency of a photodetector in responding to incident light is characterized by its responsivity (*R*). Responsivity

quantifies the photodetector's capability to convert light into electrical signals under specific bias and illumination conditions. It is defined as follows (Erdoğan et al., 2022; Daş, 2022):

$$R(A/W) = \frac{J_{ph}}{P_{in}} \quad (8)$$

where J_{ph} is the current density generated by the device and P_{in} is the total power of the light incident on the device. Figure 9 and Table 3 illustrate how the responsivity of the Fe_2O_3-G/n-Si device changes with varying applied voltage. The results indicate that the responsivity of the Fe_2O_3-G/n-Si device improves as the reverse bias voltage increases. Specifically, the responsivity is lowest at 0 V, where the device shows minimal sensitivity to light. In contrast, the responsivity reaches its highest value at -2 V, suggesting that the device becomes more efficient in converting incident light into electrical signals under higher reverse bias conditions. This behavior highlights the device's enhanced performance with increased reverse bias, which likely improves the separation and collection of photogenerated carriers, thereby increasing the overall responsivity.

Specific detectivity (*D**) is another crucial performance metric for photodiodes. It quantifies the ability of a photodiode to detect weak optical signals while minimizing noise. It is defined by the following equation (Xiong et al., 2024; Alshareefi & Al-Nafiey, 2024):

$$D^* = \frac{RA^{1/2}}{\sqrt{2qI_d}} \quad (9)$$

here, q represents the electronic charge, and A denotes the active junction area of the diode. The unit of D* is $cmHz^{1/2}W^{-1}$, commonly referred to as Jones. The calculated D* values for the fabricated device are presented in Table 4 and illustrated in Figure 10.

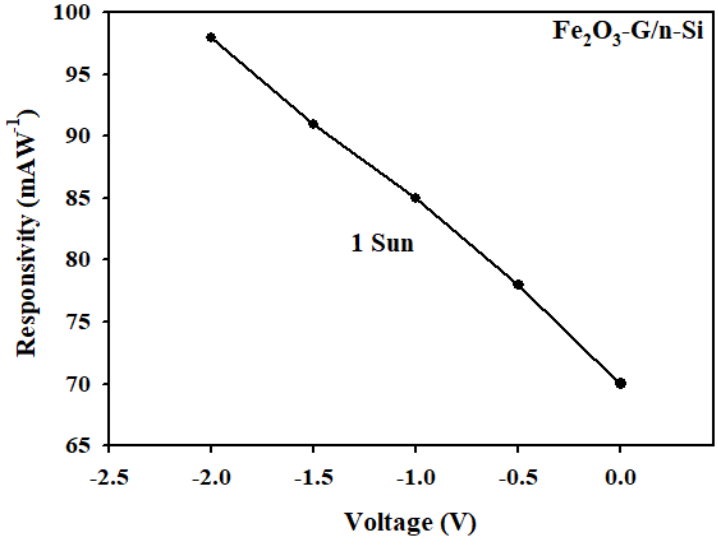

Figure 9. Variation of the responsivity of the Fe_2O_3-G/n-Si device as a function of applied voltage

Table 3. Variation in responsivity of the Fe_2O_3-G/n-Si device with different applied voltages

Device	Ambient	Responsivity (R) (mAW^{-1})				
		0V	- 0.5V	-1V	-1.5 V	-2V
Fe_2O_3-G/n-Si	1 Sun	70	78	85	91	98

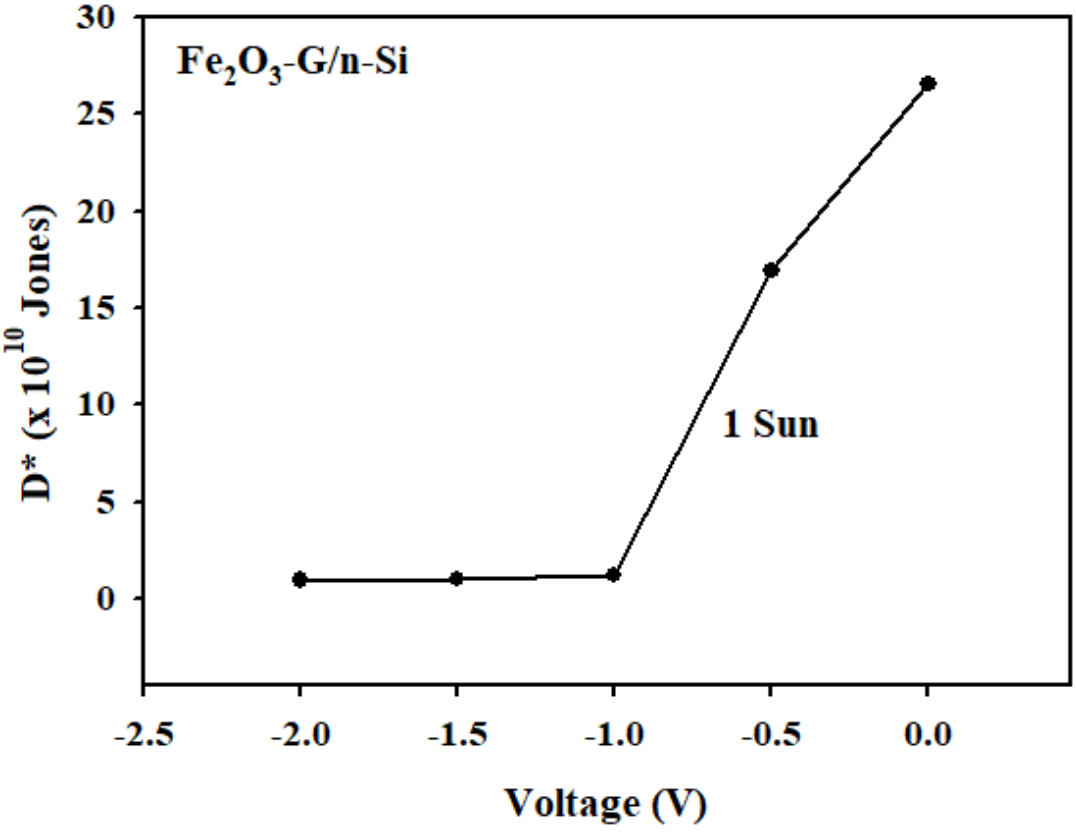

Figure 10. Dependence of D* on applied voltage for the Fe_2O_3-G/n-Si device

Table 4. Variation in D* of the Fe_2O_3-G/n-Si device with different applied voltages

Device	Ambient	Specific Detectivity (D*) (x10^{10} (Jones)				
		0V	- 0.5V	-1V	-1.5V	-2V
Fe_2O_3-G/n-Si	1 Sun	26.6	16.9	1.17	1.03	0.95

The higher the D* value, the better the photodetector is at distinguishing the signal from the noise, making it more sensitive to weak light signals. This metric is particularly important in applications where detecting faint or low-intensity light is critical. The results show that the highest D* value is achieved at 0 V, and it decreases as the reverse bias voltage increases. This behavior can be understood by considering the factors that influence D*. At 0 V, the dark current (I_d) is relatively low, which minimizes the noise in the device. Since D* is inversely proportional to the square root of the dark current (I_d), a lower dark current leads to a higher D*, indicating better sensitivity and noise performance. However, as the reverse bias voltage increases, the dark current typically increases due to enhanced carrier generation within the depletion region of the photodiode. This increase in dark current contributes to higher noise levels (shot noise), which reduces D*. Consequently, the device becomes less sensitive to weak light signals under higher reverse bias conditions. In summary, the decrease in D* with increasing reverse bias voltage is due to the rise in dark current, which introduces more noise and diminishes the photodiode's ability to detect low-intensity light efficiently.

Conclusion

In this study, Fe_2O_3-G composite material was successfully synthesized as an interlayer on n-Si substrates, and its effect on device performance was evaluated through I-V measurements. The structural and optical properties of the Fe_2O_3-G composite material were investigated through XRD, SEM/EDS, and UV-Vis spectroscopy. The obtained results confirmed that the Fe_2O_3-G composite materials were successfully synthesized. The data from XRD, SEM/EDS, and UV-Vis analyses clearly indicated the proper formation of the composite structure, along with its expected physical and optical properties. Additionally, to provide a comprehensive analysis of the electrical properties, both the Fe_2O_3-G/n-Si device and a reference

device were fabricated for comparison purposes. Both the Fe_2O_3-G/n-Si device and the reference device exhibited good rectifying characteristics, indicating their potential effectiveness in electronic applications. Key electrical parameters were determined using various methods, reinforcing the reliability of the findings. Under illumination at 1 sunlight intensity, the Fe_2O_3-G/n-Si device exhibited notable photoelectrical properties, particularly its self-powered behavior, which enables operation without an external power source. This feature demonstrates strong potential for developing efficient, self-powered photodetectors. The ability to function in remote or off-grid locations is particularly beneficial for applications such as environmental monitoring, remote sensing, and wearable electronics. By eliminating the need for external power, these devices also reduce maintenance costs and enhance sustainability, making them ideal for low-power and autonomous technologies.

Acknowledgements

The author would like to express gratitude to Nanografi Company for supplying the graphene used in this study.

Peer-review: Externally peer-reviewed.
Author Contributions: Concept –ED.; Design-ED.; Materials –GB.; Data Collection and/or Processing –ED.; Analysis and/or Interpretation –ED.; Literature Search –ED.; Writing Manuscript –ED, GB.; Critical Review –GB.
Conflict of Interest: The authors have no conflicts of interest to declare.
Financial Disclosure: The authors declared that this study has received no financial support.

Hakem Değerlendirmesi: Dış bağımsız.
Yazar Katkıları: Konsept –ED.; Tasarım -ED.; Malzemeler –GB.; Veri Toplama ve/veya İşleme –ED.; Analiz ve/veya Yorum –ED.; Literatür Taraması –ED.; Yazma –ED, GB.; Eleştirel İnceleme –GB.
Çıkar Çatışması: Yazarlar, çıkar çatışması olmadığını beyan etmiştir.
Finansal Destek: Yazarlar, bu çalışma için finansal destek almadığını beyan etmiştir.

References

Abdel-Salam, A. I., Gomaa, I., Khalid, A., & Soliman, T. S. (2022). Investigation of raman spectrum, structural, morphological, and optical features of Fe_2O_3 and Fe_2O_3/reduced graphene oxide hybrid nanocomposites. *Physica Scripta*, *97*(12), 125807. https://doi.org/10.1088/1402-4896/ac9c38

Alam, N., Ullah, A., Khan, Y., Oh, W. C., & Ullah, K. (2018). Fabrication and enhancement in photoconductive response of α -Fe_2O_3/graphene nanocomposites as anode material. *Journal of Materials Science Materials in Electronics*, *29*(20), 17786–17794. https://doi.org/10.1007/s10854-018-9886-2

Alshareefi, S. J. A., & Al-Nafiey, A. (2024). Graphene and ZnO NPs-enhanced photodetectors based on SiO NWs: Synthesis, characterization, and applications. *Results in Optics*, *16*, 100690. https://doi.org/10.1016/j.rio.2024.100690

Aydoğan, A., İncekara, M., & Türüt, A. (2010). Determination of contact parameters of Au/Carmine/n-Si Schottky device. *Thin Solid Films*, *518*(23), 7156–7160. https://doi.org/10.1016/j.tsf.2010.06.019

Bozkurt, G. (2020). Synthesis and Characterization of α-Fe_2O_3 Nanoparticles by Microemulsion Method. *Erzincan Üniversitesi Fen Bilimleri Enstitüsü Dergisi*, *13*(2), 890–897. https://doi.org/10.18185/erzifbed.742160

Can, M. M., Coşkun, M., & Fırat, T. (2012). A comparative study of nanosized iron oxide particles; magnetite (Fe_3O_4), maghemite (γ-Fe_2O_3) and hematite (α-Fe_2O_3), using ferromagnetic resonance. *Journal of Alloys and Compounds*, *542*, 241–247. https://doi.org/10.1016/j.jallcom.2012.07.091

Daş, E. (2022). Some Electrical and Photoelectrical Properties of Conducting Polymer Graphene Composite /n-Silicon Heterojunction Diode. *Sakarya University Journal of Science*, *26*(5), 1000–1009. https://doi.org/10.16984/saufenbilder.1129742

Daş, E., Incekara, U., & Aydoğan, A. (2021). A comparative study on electrical characteristics of Ni/n-Si and Ni/p-Si Schottky diodes with Pinus Sylvestris Resin interfacial layer in dark and under illumination at room temperature. *Optical Materials*, *119*, 111380. https://doi.org/10.1016/j.optmat.2021.111380

Daş, E., & Yurtcan, A. B. (2022). Synthesis of Reduced Graphene Oxide (rGO) Supported Pt Nanoparticles via Supercritical Carbon Dioxide Deposition Technique for PEM Fuel Cell Electrodes. *Journal of Anatolian Physics and Astronomy*, *1*(2), 1–17.

Erdoğan, M., Orhan, Z., & Daş, E. (2022). Synthesis of electron-rich thiophene triphenylamine based organic material for photodiode applications. *Optical Materials*, *128*, 112446. https://doi.org/10.1016/j.optmat.2022.112446

Gao, W., Li, Y., Zhao, J., Zhang, Z., Tang, W., Wang, J., Wu, Z., & Li, Z. (2022). Design and Preparation of Graphene/Fe2O3 Nanocomposite as Negative Material for Supercapacitor. *Chemical Research in Chinese Universities*, *38*(4), 1097–1104. https://doi.org/10.1007/s40242-022-1442-1

Ghobadi, A., Ghobadi, T. G. U., Karadas, F., & Ozbay, E. (2019). Semiconductor Thin Film Based Metasurfaces and Metamaterials for Photovoltaic and Photoelectrochemical Water Splitting Applications. *Advanced Optical Materials*, *7*(14). https://doi.org/10.1002/adom.201900028

Güllü, Ö., Aydoğan, Ş., & Türüt, A. (2008). Fabrication and electrical properties of Al/Safranin T/n-Si/AuSb structure. *Semiconductor Science and Technology*, *23*(7), 075005. https://doi.org/10.1088/0268-1242/23/7/075005

Gupta, R., Ghosh, K., & Kahol, P. (2009). Fabrication and electrical characterization of Au/p-Si/STO/Au contact. *Current Applied Physics*, *9*(5), 933–936. https://doi.org/10.1016/j.cap.2008.09.007

Han, L. H., Liu, H., & Wei, Y. (2011). In situ synthesis of hematite nanoparticles using a low-temperature microemulsion method. *Powder Technology*, *207*(1–3), 42–46. https://doi.org/10.1016/j.powtec.2010.10.008

Idisi, D. O., Ahia, C. C., Meyer, E. L., Bodunrin, J. O., & Benecha, E. M. (2023). Graphene oxide:Fe_2O_3 nanocomposites for photodetector applications: experimental and ab initio density functional theory study. *RSC Advances*, *13*(9), 6038–6050. https://doi.org/10.1039/d3ra00174a

Kim, S., Kim, M., & Kim, H. (2024). Self-powered photodetectors based on two-dimensional van der Waals semiconductors. *Nano Energy*, 109725. https://doi.org/10.1016/j.nanoen.2024.109725

Li, Y., & Park, C. W. (1998). Particle Size Distribution in the Synthesis of Nanoparticles Using Microemulsions. *Langmuir*, *15*(4), 952–956. https://doi.org/10.1021/la980550z

Lu, W., Guo, X., Yang, B., Wang, S., Liu, Y., Yao, H., Liu, C., & Pang, H. (2019). Synthesis and Applications of Graphene/Iron(III) Oxide Composites. *ChemElectroChem*, *6*(19), 4922–4948. https://doi.org/10.1002/celc.201901006

Middya, S., Layek, A., Dey, A., Datta, J., Das, M., Banerjee, C., & Ray, P. P. (2014). Role of zinc oxide nanomorphology on Schottky diode properties. *Chemical Physics Letters*, *610–611*, 39–44. https://doi.org/10.1016/j.cplett.2014.07.003

Muhajir, M., Puspitasari, P., & Razak, J. A. (2019). Synthesis and Applications of Hematite α-Fe2O3 : a Review. *Journal of Mechanical Engineering Science and Technology (JMEST)*, *3*(2), 51–58. https://doi.org/10.17977/um016v3i22019p051

Norde, H. (1979). A modified forward I-V plot for Schottky diodes with high series resistance. *Journal of Applied Physics*, *50*(7), 5052–5053. https://doi.org/10.1063/1.325607

Orhan, Z., Cinan, E., Çaldıran, Z., Kurucu, Y., & Daş, E. (2020). Synthesis of CuO–graphene nanocomposite material and the effect of gamma radiation on CuO–graphene/p-Si junction diode. *Journal of Materials Science Materials in Electronics*, *31*(15), 12715–12724. https://doi.org/10.1007/s10854-020-03823-8

Ramakrishnan, K., Ajitha, B., & Reddy, Y. a. K. (2023). Review on metal sulfide-based nanostructures for photodetectors: From ultraviolet to infrared regions. *Sensors and Actuators. A, Physical*, *349*, 114051. https://doi.org/10.1016/j.sna.2022.114051

Saleem, S., Ashiq, M. N., Manzoor, S., Ali, U., Liaqat, R., Algahtani, A., Mujtaba, S., Tirth, V., Alsuhaibani, A. M., Refat, M. S., Ali, A., Aslam, M., & Zaman, A. (2023). Analysis and characterization of opto-electronic properties of iron oxide (Fe_2O_3) with transition metals (Co, Ni) for the use in the photodetector application. *Journal of Materials Research and Technology*, *25*, 6150–6166. https://doi.org/10.1016/j.jmrt.2023.07.065

Sarkar, K., & Kumar, P. (2024). Nanostructured carbon heterojunctions for broadband photodetection: Development roadmap, emerging technologies, and future perspectives. *Carbon*, *219*, 118842. https://doi.org/10.1016/j.carbon.2024.118842

Sun, M., Liu, H., Liu, Y., Qu, J., & Li, J. (2015). Graphene-based transition metal oxide nanocomposites for the oxygen reduction reaction. *Nanoscale*, *7*(4), 1250–1269. https://doi.org/10.1039/c4nr05838k

Talebi, S., & Eshghi, H. (2023). Achievement of high infrared photoresponse in n-MoO_3/p-Si heterostructure photodiode prepared via the thermal oxidation method, the influence of oxygen flow rate. *Materials Chemistry and Physics*, *303*, 127792. https://doi.org/10.1016/j.matchemphys.2023.127792

Wang, S., Liu, H., Cao, Z., Wang, X., Zhang, L., Ding, J., Xue, Y., Han, T., Li, F., Shan, L., & Long, M. (2023). Highly Sensitive Long-Wave Infrared Photodetector Based on Two-Dimensional Hematite α-Fe2O3. *Advanced Optical Materials*, *11*(19). https://doi.org/10.1002/adom.202300382

Xiong, G., Zhang, G., & Feng, W. (2024). High performance photodetectors by integrating CsPbBr3 perovskite directly on the germanium wafer. *Materials Research Bulletin*, *179*, 112959. https://doi.org/10.1016/j.materresbull.2024.112959

Yildirim, G. B., & Daş, E. (2023). The synthesis of MgO and MgO-graphene nanocomposite materials and their diode and photodiode applications. *Physica Scripta*, *98*(8), 085911. https://doi.org/10.1088/1402-4896/ace249

Yurtcan, A. B., & Daş, E. (2018). Chemically synthesized reduced graphene oxide-carbon black based hybrid catalysts for PEM fuel cells. *International Journal of Hydrogen Energy*, *43*(40), 18691–18701. https://doi.org/10.1016/j.ijhydene.2018.06.186